AIMS Materials Science, 7(2): 192–202.
DOI:10.3934/matersci.2020.2.192
Received: 07 February 2020
Accepted: 13 May 2020
Published: 22 May 2020

http://www.aimspress.com/journal/Materials

Research article

Microstructures, mechanical properties, and corrosion behavior of novel multi-component Ti–6Mo–6Nb–xSn–xMn alloys for biomedical applications

Cahya Sutowo[1], Galih Senopati[2], Andika W Pramono[2], Sugeng Supriadi[3] and Bambang Suharno[1,*]

[1] Department of Metallurgy and Material Engineering, Faculty of Engineering Universitas Indonesia, Depok 16424, Indonesia
[2] Research Center for Metallurgy and Materials Indonesian Institute of Sciences Tangerang Selatan 15314, Indonesia
[3] Department of Mechanical Engineering, Faculty of Engineering, Universitas Indonesia, Depok 16424, Indonesia

* **Correspondence:** Email: suharno@metal.ui.ac.id; Tel: +62217863510.

Abstract: In this study, novel multi-component Ti–Mo–Nb–Sn–Mn alloys were developed as a solution to the mismatch in elastic moduli of implant and human bone and toxicity of the Ti–6Al–4V alloy commonly used in the biomedical field. This study is aimed to investigate the effects of Sn and Mn addition as beta stabilizers on the microstructural transformation, mechanical properties, and corrosion behavior of the alloys. Ti–6Mo–6Nb–xSn–xMn (x = 0, 4, or 8) alloys were re-melted five times in an arc re-melting process under an argon atmosphere and the obtained ingots were characterized using optical microscopy, X-ray diffractometry, ultrasound, a Vicker's hardness tester, and polarization tests in a Ringer solution. The results show that a Ti–6Mo–6Nb–xSn–xMn alloy had a lower elastic modulus and better corrosion resistance than those of commercial Ti–6Al–4V alloy, making it a potential candidate for use in the biomedical field.

Keywords: multi-component beta alloy; Ti–6Mo–6Nb–xSn–xMn; elastic modulus; corrosion resistance

1. Introduction

Although scientific developments and economic growth of a country generally lead to an improvement in the quality of life of its population [1], they may also have a negative impact. For instance, there is an increased need for implant materials that can be used to replace failed body tissues to improve the quality of life of the patients requiring the implant. Around 70–80% of the implants used in the biomedical field are made from metallic materials [2], which have been the case since the beginning of the industrial revolution in the 19th century [3], and these material are now widely used in orthopedic devices such as bone plates, pins, screws, and total joint replacements [4]. Due to their high strength and toughness under loading conditions, metallic implants have better properties than other implant materials, such as ceramics and polymers [5]. However, metallic implants are sometimes toxic and lack corrosion resistance [6]. Compared with metallic materials such as cobalt alloys and steel, titanium shows better corrosion resistance and biocompatibility with the human body [7,8]. Ti–6Al–4V alloy has been widely used in the biomedical fields due to its highly specific strength, good corrosion resistance and biocompatibility [9].

Vanadium has been reported as having cytotoxic effects in the human body, and aluminum is thought to contribute toward Alzheimer's disease [10]. Moreover, the large difference in the elastic modulus of human bone and Ti–6Al–4V may result in a stress shielding effect and, thus, promote implant failure [11]. Stress shielding is a phenomenon that takes place when the load in the area of the implanted material is entirely supported by the implant material, so that the bones around the implanted material are lack in nutrient intake [12]. When this happens over a long period of time, the bone around the area of the implant loses its mass, resulting in the failure of the implant due to the fragility of the surrounding bone [13].

The β-type titanium alloy has been developed with a lower elastic modulus than that of the Ti–6Al–4V alloy to reduce stress shielding effect [14]. The β-phase has been prepared via heat treatment, so it retains its full β-phase upon going from a high (β-phase field) to room temperature [15], which is possibly due to the addition of a sufficient amount of beta stabilizing elements to suppress the growth of α' and α" phases usually formed at room temperature [16–18]. In 1996, the first β-type titanium alloy, Ti–13Nb–13Zr, was developed by Mishra, with the later development of a β-type titanium alloy using the low-cost β stabilizing elements Mn, Sn, Fe, and Cr [19–21].

Lately, there has been focus on developing a non-toxic β-type titanium alloy with a low elastic modulus. So far, a β-type titanium alloy, Ti–Nb–Ta–Zr, has been found to have the lowest elastic modulus approaching that of human bone [22]. Gabriel developed a Ti–12Mo–3Nb alloy aimed at reducing the use of Ta and Nb, however, a relatively high elastic modulus of 105 GPa was achieved [23].

Some author stated that Sn is neutral element since it has no influence on both α or β phase boundary. However, Morinaga stated that Sn and other element (O, Al, and Zr) can behave like β stabilizer. And from Mello's studies of Ti–Mo–Sn and Zhang studies of Ti–7.5Nb–4Mo–xSn reported that Sn has influence on supressed ω phase formation and could reduce the elastic modulus [16,24]. When 6% Sn was added to the Ti–8Mo alloy, the full beta-phase formed an elastic modulus of around 78 GPa [16]. Moreover, Santos also developed a beta titanium alloy containing Mn as a beta stabilizer known as a common alloying element. It was reported that at a Mn content of 9%, the lowest elastic modulus value was achieved at 94 GPa, and after this content, a full beta-phase of the binary Ti–Mn alloy formed [25]. Several studies using cheap metal with a lower density

did not result in the formation of a beta titanium alloy with an elastic modulus approaching that of a human bone. This study accommodates the use of titanium alloy with various combinations of low cost alloying elements (multi-components).

The addition of stannum and manganese, as both are low-cost elements, is to replace tantalum and reduce the use of niobium and molybdenum as beta-phase stabilizers. In this study, beta-phase titanium alloys were synthesized using Mo, Nb, Sn, and Mn as alloying elements, with the aim of determining the effects of adding Sn and Mn on a multi-component Ti–6Mo–6Nb–4Sn–xMn (x = 0, 4, or 8 wt%) and Ti–6Mo–6Nb–8Sn–xMn (x = 0, 4, or 8 wt%) alloys with respect to their phases, mechanical properties, and electrochemical properties in a Ringer solution.

2. Materials and methods

Multi-component β-type Ti–Mo–Nb–Sn–Mn (wt%) alloys were synthesized using Ti (99.9% pure), Nb (99.5% pure), Mo (99.5% pure), Sn (99.5% pure), and Mn (99.5% pure) from Nilaco Japan as raw materials. An arc melting furnace with a non-consumable tungsten electrode on a water-cooled copper hearth was used to melt the alloys under an ultra-high purity argon atmosphere. Before melted in a vacuum arc furnace, the raw materials were prepared by cutting them to the applicable sizes, cleaning them using volatile organic solvents, and subsequently weighing them according to the calculation of material balance, and loading them onto the top of a copper crucible in the melting chamber. The melting process took place under vacuum that is achieved by pumping the chamber up to the vacuum condition and subsequently draining it by argon, so that the melting chamber is free of oxygen. The ingots were re-melted five times to ensure the process had undergone completion rather than to improve their chemical homogeneity. The ingot was further homogenized by heating in a tube furnace with an argon atmosphere at 1150 °C for 6 h, followed by water quench cooling.

The chemical compositions of the as-cast samples were examined by Rigaku X-ray fluorescence spectroscopy (XRF). The as-cast Ti–Mo–Nb–Sn–Mn was sectioned using an abrasive cutting wheel with dimensions of 2 cm × 2 cm × 1 cm. Samples for microstructure analysis were sanded on different 80–1500 grade SiC paper, polished with alumina paste, and etched using a solution of Kroll's reagent containing 2 mL HF + 6 mL of HNO_3 + 92 mL of H_2O. The microstructures of the samples were observed using a Meiji optical microscope. Powder X-ray diffraction (XRD) measurements were carried out at room temperature to analyses their phases using a Rigaku diffractometer equipped with a CuKα radiation source, operating at 30 kV and 15 mA. Vicker's hardness measurements were performed using a Mitutoyo hardness tester with a 0.3 N load for a 12 s indentation, and the elastic modulus were measured using an ultrasonic method according to an ASTM-E494-95 standard [26,27]. Square Ti–Mo–Nb–Sn–Mn alloy samples were cut to a size of 0.5 cm^2 for electrochemical testing purposes, and their surfaces polished with fine 1200 grade SiC paper. The electrochemical measurement were performed on autolab 302 Multi BA electrochemical working station. The tests were carried out in a three electrode corrosion cell: Ag–AgCl as the reference electrode, platinum wire as the counter electrode, as well as working electrode. Tests were carried out in Ringer's solution at neutral pH and room temperature. The potentiodynamic polarization curve was recorder at scan rate of 0.5 mV/s.

3. Results and discussion

Table 1 shows the chemical compositions of the Ti–Mo–Nb–Sn–Mn ingots after being re-melted five times in an arc re-melting furnace under an argon atmosphere, the results show that the measured compositions are close to the ideal compositions.

Table 1. Chemical compositions of the As-cast Ti–Mo–Nb–Sn–Mn alloys.

Alloy	Composition				
	Mo (wt%)	Nb (wt%)	Sn (wt%)	Mn (wt%)	Ti (wt%)
Ti–6Mo–6Nb–4Sn	5.95	6.16	4.22	-	Bal.
Ti–6Mo–6Nb–4Sn–4Mn	5.55	5.58	4.57	3.30	Bal.
Ti–6Mo–6Nb–4Sn–8Mn	5.39	5.50	4,61	7.58	Bal.
Ti–6Mo–6Nb–8Sn	5.80	5.21	7.91	-	Bal.
Ti–6Mo–6Nb–8Sn–4Mn	5.02	5.47	8.25	4.07	Bal.
Ti–6Mo–6Nb–8Sn–8Mn	5.02	5.80	7.96	7.36	Bal.

Figure 1 shows the XRD patterns of the as-cast Ti–Mo–Nb–Sn–Mn alloys, where the profiles of the quaternary Ti–6Mo–6Nb–4Sn and Ti–6Mo–6Nb–8Sn alloys show the existence of α and β phases of titanium. Meanwhile, only the β-phase was observed inquinary Ti–Mo–Nb–Sn–Mn alloys. The diffraction pattern with the α-phase peak indicated that the alloy has an HCP crystal structure with α(101). From Figure 1, it can be seen that the α-phase in the alloys containing 0% Mn exhibit peaks with 2θ-angle positions of 35.6°, 40.5°, 53°, 63°, and 76°. The titanium α-phase peak disappeared after Mn is added. Since Mn is β-phase stabilizer, its addition resulted in the full β-phase alloy with body center cubic crystal structure at the orientations of (110), (200), (211), and (220). The β-phase was detected at peaks of 39.5°, 56.9°, 70.5°,85° and 96°.

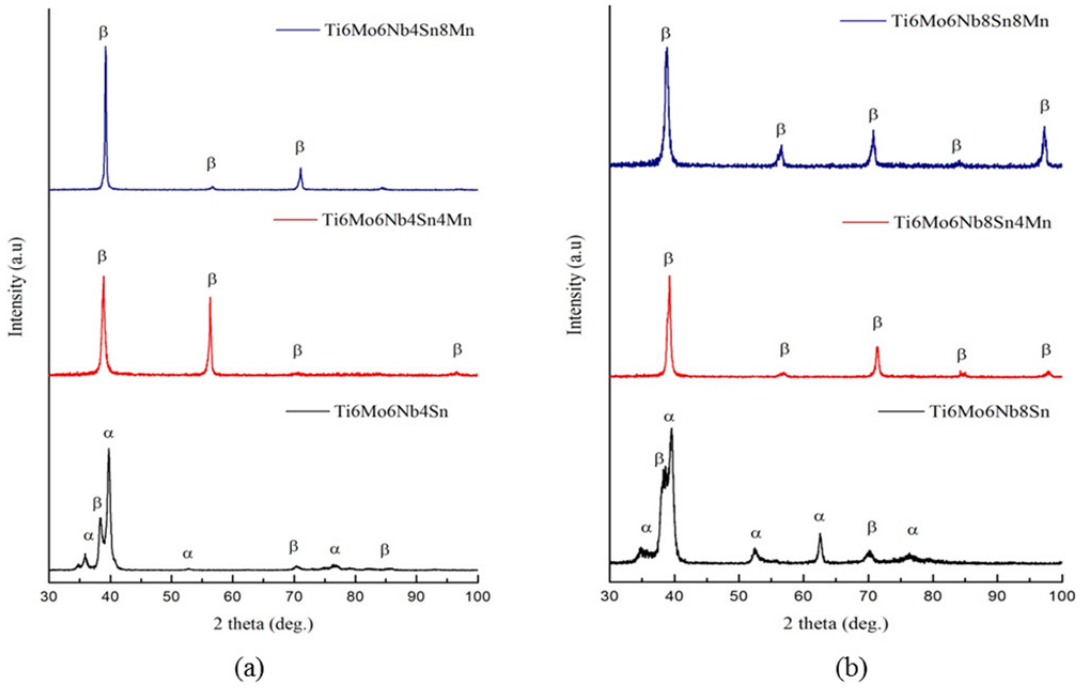

Figure 1. Diffraction patterns of the Ti–Mo–Nb–Sn–Mn alloys.

Moreover, Figure 1 shows that adding Mn has a positive impact on the phase constituent formation in the titanium alloys. Prior to Mn addition, the α phase still existed, and then disappeared when Mn was added to the Ti–6Mo–6Nb–4Sn and Ti–6Mo–6Nb–8Sn alloys. It was previously reported by Wang that only the β phase was observed when 5% Sn was added to a Ti–16Nb alloy [28]. Chen also reported that the α phase disappeared when 3% Mn was added to a Ti–16Nb alloy, leading to an increase in the β phase content [29].

Figure 2 shows optical microscope images of the microstructures of Ti–Mo–Nb–Sn–Mn alloys synthesized involving five-cycle melting process. The Figure 2a–f show that the β-phase titanium has equiaxed grain shapes. Upon the addition of 4% Mn increased the grain size of the β-phase titanium slightly. Increases Mn content up 8% Mn reduce the grain size to 100–200 μm long grain. Macro segregation or micro segregation was not observed in the melted samples, which negatively affected the mechanical properties of the alloys. Santos reported the increase in Ti–xMn grain size when 18% of Mn was added [25]. This phenomenon may be caused by the stability of β phase reaching a critical point marked by a decrease in beta transus temperature leading to the grain growth occur. The various content of Sn does not have a significant effect on the grain size. This phenomenon was also reported by Wang where grain size in titanium alloy Ti–Nb–Sn was relatively the same as polygon-shaped grains [28].

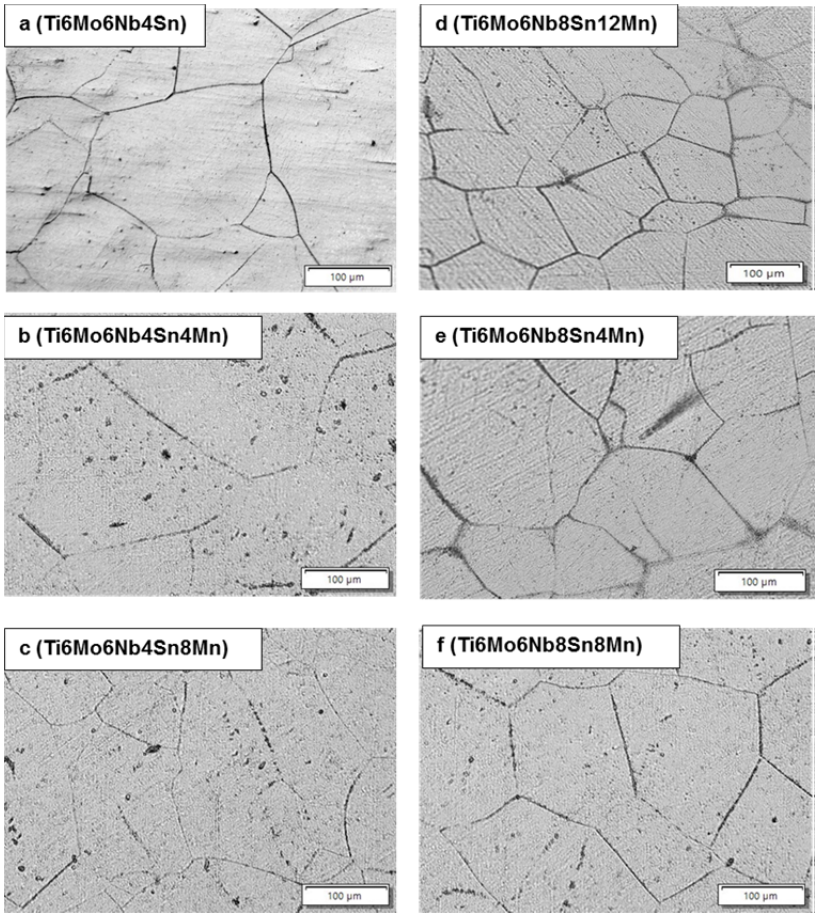

Figure 2. Optical microscope images of the As-cast Ti–Mo–Nb–Sn–Mn alloys: (a) Ti–6Mo–6Nb–4Sn, (b) Ti–6Mo–6Nb–4Sn–4Mn, (c) Ti–6Mo–6Nb–4Sn–8Mn, (d) Ti–6Mo–6Nb–8Sn, (e) Ti–6Mo–6Nb–8Sn–4Mn, and (f) Ti–6Mo–6Nb–8Sn–8Mn.

Figure 3 shows a plot of the Vicker's microhardness values of the Ti–Mo–Nb–Sn–Mn alloys synthesized using five-cycle melting process, it can be observed that the addition of Mn changes the hardness values of the Ti–Mo–Nb–Sn–Mn alloys. Prior to the addition of Mn, the hardness value of Ti–6Mo–6Nb–4Sn was 327 HV, which then decreased to 318 HV after the addition of 4% Mn. This decrease in the hardness values of the Ti–6Mo–6Nb–4Sn alloy upon the addition of Mn resulted from changes in the grain size of the β phase of the Ti–6Mo–6Nb–4Sn–xMn alloy. The finer the grain size of the β-phase titanium is, the higher the hardness value of Ti–6Mo–6Nb–4Sn–xMn is. However at 8% Mn and Sn, the hardness of the alloy increased indicating that the Sn and Mn addition have strong solid-solution hardening effect [24].

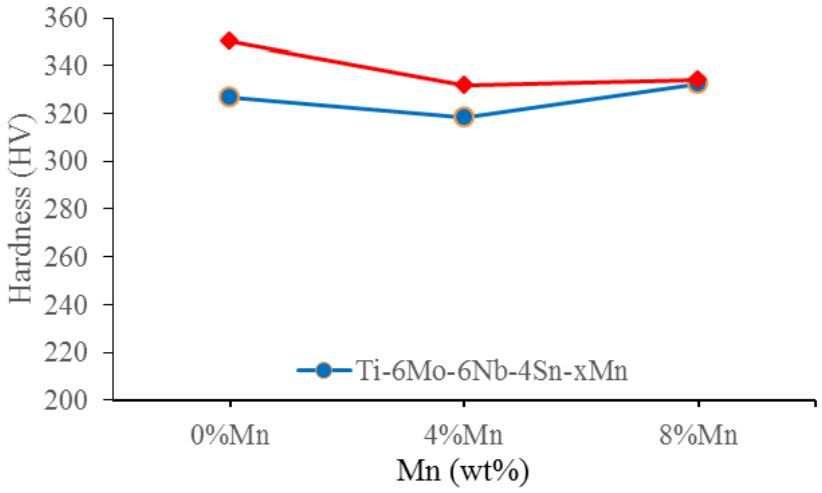

Figure 3. Vicker's hardness values of the Ti–Mo–Nb–Sn–Mn alloys according to their Mn content.

The hardness value of Ti–6Mo–6Nb–8Sn–xMn decreased when 4% Mn was added due to an increase in the grain size of the β-phase in the alloy, as shown in Figure 2d,e. However, 4% Mn was not sufficient enough to retain the grain growth in the β phase with higher Sn content (8% Sn). As the Mn content was increased to 8%, it began to suppress the grain growth in the β phase, as shown in Figure 2f, leading to a slight increase in the hardness value of the Ti–6Mo–6Nb–8Sn–8Mn alloy.

The hardness value is influenced by the phase constitutent of its alloy and the microstructure (phase and grain size). In Figure 2 the grain size of Ti–6Mo–6Nb–4Sn–8Mn and Ti–6Mo–6Nb–8Sn-8Mn were nearly same in size, and from the XRD pattern both alloys only contained β phase (no α phase observed). This may cause the hardness value of both Ti–6Mo–6Nb–4Sn–8Mn and Ti–6Mo–6Nb–8Sn–8Mn to be relatively the same.

It was also found that further addition of Mn affected the change in the elastic modulus value of the Ti–6Mo–6Nb–4Sn alloy, as shown in Figure 4. The elastic modulus of the Ti–6Mo–6Nb–4Sn alloy was 103 GPa, then decreased to 94 GPa upon the addition of 4% Mn. The elastic modulus of the Ti–6Mo–6Nb–8Sn alloy decreased from 98 to 92 GPa with the addition of 4% Mn. Moreover, changes in the volume fractions of α and β phase titanium also resulted in changes to the elastic modulus of the titanium alloys, where α-phase titanium has a higher elastic modulus than that of the β-phase titanium, with the order of elastic modulus values following: $\beta < \alpha'' < \alpha' < \acute{\omega}$ [27].

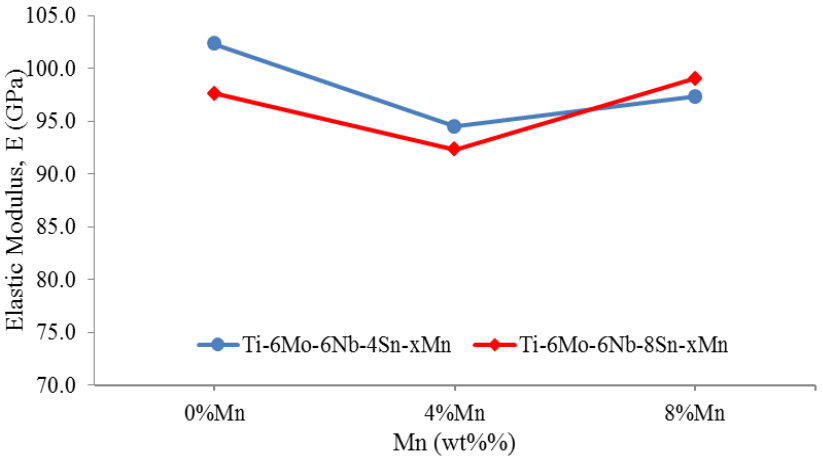

Figure 4. Elastic modulus of the Ti–Mo–Nb–Sn–Mn alloys according to their Mn content.

In terms of the Ti–6Mo–6Nb–4Sn alloy, its grain size increased along with the Mn content (see Figure 2a–c), resulting in increases in the strength, elastic modulus, and hardness of the alloy in line with the Hall–Petch equation. For the Ti–6Mo–6Nb–8Sn alloy, a small amount of the β-phase formed (Figure 1) leading to decrease in its elastic modulus with respect to that of the Ti–6Mo–6Nb–4Sn alloy (Figure 4). However, as the Mn content of the Ti–6M–6Nb–8Sn alloy was increased, some intermetallic Mn–Sn compounds may have precipitated within the grains in the form of Mn_3Sn, Mn_3Sn_2, $MnSn_2$, or $Mn_{(2-x)}Sn$. These precipitates significantly hinder the mobility of dislocations, leading to an increase in the elastic modulus [30]. Compared to α-β type titanium alloys, the elastic modulus of the Ti–6Mo–6Nb-based titanium alloy is still lower than that of the Ti–6Al–4V alloy,the value of which is 115 GPa, and a β-type Ti–12Mo–3Nb (105 GPa) alloy [23,27].

Figure 5 shows a polarization curve of the corrosion test results of the Ti–Mo–Nb–Sn–Mn alloys in Ringer solution simulating human body fluid. Many corrosion tests were carried out on commercial Ti–6Al–4V alloy in the same solution. It was observed that both Ti–6Mo–6Nb–4Sn–xMn and Ti–6Mo–6Nb–8Sn–xMn alloys had similar and typical passive behaviors, indicating the formation of passive film on the surface of Ti–Mo–Nb–Sn–Mn alloys

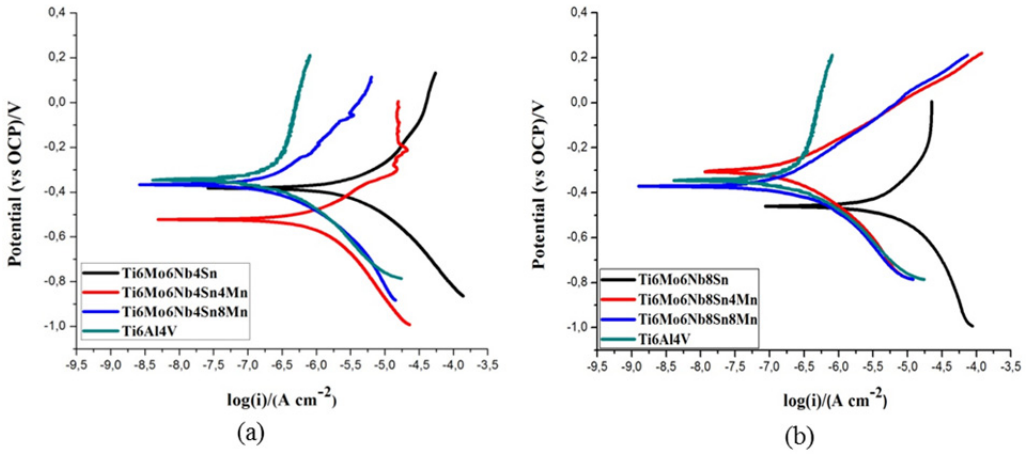

Figure 5. Potentiodynamic polarization curves of Ti–Mo–Nb–Sn–Mn in the Ringer solution.

Potentiodynamic polarization tests were carried out in the range of −1000 mV to +200 mV versus OCP for all alloys. The parameters of corrosion, corrosion potential (E_{Corr}) and corrosion current density (i_{corr}) were obtained from the tafel area. The corrosion current represents the degree of degradation of the alloy and is used to determine the corrosion rate of the alloy. Different passive areas were observed on the anodic polarization curves, of wich the formation of passive films occurs. Corrosion rate was calulated from the corrosion current density using the equation according to ASTM Standard G102-89 [31].

Table 2 summarized the electrochemical parameters, such as corrosion potential (E_{corr}) and corrosion current density (I_{corr}) of Ti–Mo–Nb–xSn–xMn alloys in Ringer solution. The I_{corr} of the alloys prior to Mn addition showed the values of 3.162 and 5.010 μA/cm^2. The I_{corr} value subsequently decreased with increasing of Mn content. The potentiodynamic corrosion test data shown in Table 2 also provide evidence that the Ti–6Mo–6Nb–4Sn–4Mn, Ti–6Mo–6Nb–4Sn–8Mn, Ti–6Mo–6Nb–8Sn–4Mn, and Ti–6Mo–6Nb–8Sn–8Mn alloys have better corrosion resistance than that of the commercial Ti–6Al–4V in the Ringer solution, with the Ti–6Mo–6Nb–8Sn–4Mn alloy showing the lowest corrosion rate of 0.0016 mm per year (mmpy). Tsao reported that adding Sn to a Ti–7Cu titanium alloy increased its corrosion resistance in NaCl solution [32]. He also carried out energy-dispersive X-ray spectroscopic (EDS) tests to determine the elements present in the alloys after the potentiodynamic corrosion tests, where the results showed the formation of a passive layer in the form of TiO, CuO, and SnO on the surface of a Ti–Cu–Sn alloy [32]. In a heat-treated AZ91 magnesium alloy, additional Mn increased the corrosion potential, lowered the corrosion current density, and reduced the corrosion rates, similar to what has been observed in Ti–Mo–Nb–Sn–Mn alloys [33].

Table 2. Corrosion parameters of the Ti–6Mo–6Nb–xSn–xMn alloy in the Ringer solution.

Alloy	Corrosion potential E_{corr} ($V_{Ag/AgCl}$)	Corrosion current density I_{corr} (μA/cm^2)	Corrosion rate (mmpy)
Ti–6Mo–6Nb–4Sn	−0.383	3.162	0.04934
Ti–6Mo–6Nb–4Sn–4Mn	−0.522	0.633	0.00972
Ti–6Mo–6Nb–4Sn–8Mn	−0.367	0.131	0.00198
Ti–6Mo–6Nb–8Sn	−0.461	5.010	0.07838
Ti–6Mo–6Nb–8Sn–4Mn	−0.306	0.112	0.00160
Ti–6Mo–6Nb–8Sn–8Mn	−0.372	0.127	0.00163
Ti–6Al–4V	−0.350	0.316	0.00504

4. Conclusions

The Mn and Sn addition had a positive impact on the formation of β-phase titanium in Ti–Mo–Nb–Sn–Mn alloy and reduced α-phase formation in the β-phase matrix. Due to the reduction of α-phase content, sample hardness and elastic modulus of β-phase alloy were lower than that of α-β titanium alloy. Moreover, the alloys with stood the formation of α-phase titanium. The higher the Mn and Sn content, the lower the amount of α-phase titanium, and the more β-phase titanium were formed. The addition of 4% Mn to this alloy led to the formation of full β-phase titanium with an optimum modulus of elasticity of 92 GPa. It is suggested that the further addition of Mn enhances the corrosion resistance of Ti–6Mo–6Nb–8Sn alloys. The optimum corrosion rate of this alloy was also achieved upon the addition of 4% Mn. To ensure the biocompatibility of these alloys, further studies

should be conducted to determine the optimum Mn content without sacrificing the balance of the mechanical properties and corrosion resistance in various simulated body fluids.

Acknowledgements

We would like to thank Directorate of Researches and Community Service, Universitas Indonesia (DRPM UI) for their financial support through the TADok grant funds with the contract number NKB-0155/UN2.R3.1/HKP.05.00/2019 and for helping us conduct this study.

Conflicts of interests

All authors declare no conflicts of interest in this paper.

References

[1] Park JB (1984) *Biomaterials Science and Engineering*, Boston: Springer.
[2] Niinomi M, Nakai M, Hieda J (2012) Development of new metallic alloys for biomedical applications. *Acta Biomater* 8: 3888–3903.
[3] Chen Q, Thouas GA (2015) Metallic implant biomaterials. *Mat Sci Eng R* 87: 1–57.
[4] Geetha M, Singh AK, Asokamani R, et al. (2009) Ti based biomaterials, the ultimate choice for orthopaedic implants—A review. *Prog Mater Sci* 54: 397–425.
[5] He G, Hagiwara M (2006) Ti alloy design strategy for biomedical applications. *Mat Sci Eng C-Mater* 26: 14–19.
[6] Li Y, Yang C, Zhao H, et al. (2014) New developments of Ti-based alloys for biomedical applications. *Materials* 7: 1709–1800.
[7] Hsu H, Wu S, Hsu S, et al. (2013) The structure and mechanical properties of as-cast Ti–25Nb–xSn alloys for biomedical applications. *Mat Sci Eng A-Struct* 568: 1–7.
[8] Plecko M, Sievert C, Andermatt D, et al. (2012) Osseointegration and biocompatibility of different metal implants-a comparative experimental investigation in sheep. *BMC Musculoskel Dis* 13: 32.
[9] Rack HJ, Qazi JI (2006) Titanium alloys for biomedical applications. *Mat Sci Eng C-Mater* 26: 1269–1277.
[10] GepreelMA, Niinomi M (2013) Biocompatibility of Ti-alloys for long-term implantation.*J MechBehav Biomed* 20: 407–415.
[11] Senopati G, Sutowo C, Kartika I, et al. (2019) The effect of solution treatment on microstructure and mechanical properties of Ti–6Mo–6Nb–8Sn alloy. *Mater Today* 13: 224–228.
[12] Davis JR (2003) *Handbook of Materials for Medical Devices*. Ameriacan: ASM International-Materials Park.
[13] Ballo A, Moritz N (2010) Biomechanics concepts of bone-oral implan interface, In: Levy JH, *Biomechanics: Principles, Trends, and Applications*, New York: Nova Science Publisher, 117.
[14] Mohammed MT, Khan ZA, Siddiquee AN (2014) Beta titanium alloys: the lowest elastic modulus for biomedical applications: a review. *Int J Chem Mol Nucl Mater Metall Eng* 8: 726–731.
[15] Kolli RP (2018) A review of metastable beta titanium alloys. *Metals* 8: 1–41.

[16] De Mello MG, Salvador CF, Cremasco A, et al. (2015) The effect of Sn addition on phase stability and phase evolution during aging heat treatment in Ti–Mo alloys employed as biomaterials. *Mater Charact* 110: 5–13.
[17] Xu L, Xiao S, Tian J, Chen Y (2013) Microstructure, mechanical properties and dry wear resistance of β-type Ti–15Mo–xNb alloys for biomedical applications. *T Nonferr Metal Soc* 23: 692–698.
[18] Lu J, Zhao Y, Ge P, et al. (2013) Microstructure and beta grain growth behavior of Ti–Mo alloys solution treated. *Mater Charact* 84: 105–111.
[19] Cho K, Niinomi M, Nakai M, et al. (2016) Improvement in mechanical strength of low cost beta type Ti–Mn alloys fabricated by metal injection molding through cold rolling. *J Alloy Compd* 664: 272–283.
[20] Markovs PE, Ikeda M (2013) Influence of alloying elements on the aging of economically alloyed metastable titanium beta alloy. *Mater Sci* 49: 78–84.
[21] Ehtemam-Haghighi S, Cao G, Zhang LC (2016) Nano indentation study of mechanical properties of Ti based alloys with Fe and Ta additions. *J Alloy Compd* 692: 892–897.
[22] Narita K, Niinomi M, Nakai M, et al. (2012) Development of thermo-mechanical processing for fabricating highly durable β-type Ti–Nb–Ta–Zr rod for use in spinal fiation devices. *J Mech Behav Biomed* 9: 207–216.
[23] Gabriel SB, Panaino JVP, Santos ID, et al. (2012) Characterization of a new beta titanium alloy Ti–12Mo–3Nb for biomedical applications. *J Alloy Compd* 536: S208–S210.
[24] Zhang DC, Yang S, Wei M, et al. (2012) Effect of Sn addition on the microstructure and superelasticity in Ti–Nb–Mo–Sn alloys. *J Mech Behav Biomed* 13: 156–165.
[25] Santos PF, Niinomi M, Cho K, et al. (2015) Microstructures, mechanical properties and cytotoxicity of low cost beta Ti–Mn alloys for biomedical applications. *Acta Biomater* 26: 366–376.
[26] ASTM International (1995) Standard practice for measuring ultrasonic velocity in materials. ASTM E494-95. Avaliable from: https://www.astm.org/DATABASE.CART/HISTORICAL/E494-95.htm.
[27] Majumdar P, Singh SB, Chakraborty M (2008) Elastic modulus of biomedical titanium alloys by nano-indentation and ultrasonic techniques—A comparative study. *Mater Sci Eng A-Struct* 489: 419–425.
[28] Wang BL, Zheng YF, Zhao LC (2008) Effects of Sn content on the microstructure, phase constitution and shape memory effect of Ti–Nb–Sn alloys. *Mater Sci Eng A-Struct* 486: 146–151.
[29] Chen Z, Liu Y, Jiang H, et al. (2017) Microstructures and mechanical properties of Mn modified Ti–Nb-based alloys. *J Alloy Compd* 723: 1091–1097.
[30] Aljarrah M, Obeidat S, Fouad RH, et al. (2015) Thermodynamic calculations of the Mn–Sn, Mn–Sr and Mg–Mn–{Sn, Sr} systems. *IET Sci Meas Technol* 9: 681–692.
[31] ASTM International (1999) Standard practice for calculation of corrosion rates and related information from electrochemical measurements. ASTM G102-89. Avaliable from: https://www.astm.org/DATABASE.CART/HISTORICAL/G102-89R99.htm
[32] Tsao LC (2015) Effect of Sn addition on the corrosion behavior of Ti–7Cu–Sn cast alloys for biomedical applications. *Mater Sci Eng C-Mater* 46: 246–252.

[33] Li XY, Li MZ, Fan LQ, et al. (2014) Effects of Mn on corrosion resistant property of AZ91 alloys. *Rare Metal Mater Eng* 43:278–282.

AIMS Press